AGU PUBLICATIONS

Geophysical Research Letters

RESEARCH LETTER

10.1002/2016GL072229

Key Points:
- A coupled 25–30 year mode is present in the ocean-atmosphere system
- This coupled mode is useful in extended-range prediction
- The strength of the coupling and the predictability vary with the seasons

Supporting Information:
- Supporting Information S1

Correspondence to:
S. Vannitsem,
svn@meteo.be

Citation:
Vannitsem, S., and M. Ghil (2017), Evidence of coupling in ocean-atmosphere dynamics over the North Atlantic, *Geophys. Res. Lett.*, *44*, 2016–2026, doi:10.1002/2016GL072229.

Received 7 DEC 2016
Accepted 11 JAN 2017
Accepted article online 14 JAN 2017
Published online 22 FEB 2017

Evidence of coupling in ocean-atmosphere dynamics over the North Atlantic

Stéphane Vannitsem[1] **and Michael Ghil**[2,3]

[1]Royal Meteorological Institute of Belgium, Brussels, Belgium, [2]Geosciences Department and Laboratoire de Météorologie Dynamique (CNRS and IPSL), École Normale Supérieure and PSL Research University, Paris, France, [3]Department of Atmospheric and Oceanic Sciences and Institute of Geophysics and Planetary Physics, University of California, Los Angeles, California, USA

Abstract Coupling between the ocean and the atmosphere is investigated in reanalysis data sets. Projecting the data sets onto a dynamically defined subspace allows one to isolate the dominant modes of variability of the coupled system. This coupled projection is then analyzed using multichannel singular spectrum analysis. The results suggest that a dominant low-frequency signal with a 25–30 year period already mentioned in the literature is a common mode of variability of the atmosphere and the ocean. A new score for evaluating the internal nature of the common variability is then introduced, and it confirms the presence of coupled dynamics in the ocean-atmosphere system that impacts the atmosphere at large scale. The physical nature of this coupled dynamics is then discussed.

1. Introduction

The investigation of low-frequency variability (LFV) in the midlatitude atmosphere, for instance of the North Atlantic Oscillation (NAO), is currently attracting considerable interest [e.g., *Bladé et al.*, 2011; *Hurrell et al.*, 2013, and references therein]. One of the main reasons is LFV's potential to enable predictions beyond the generally accepted upper bound of weather forecasting skill of 10–15 days in midlatitudes [cf. *Baehr et al.*, 2015; *Kadow et al.*, 2015; *Maidens et al.*, 2013; *Menary et al.*, 2015]. As illustrated in the latter works, attaining this goal is challenging and it still requires better understanding how the atmosphere and the ocean interact with each other at midlatitudes. The answer to this fundamental question is hampered by the mismatch between the time and space scales of the two subsystems.

To understand the coupled system's dynamics, the usual strategy is to analyze the one-way sensitivity of either component to forcing by the other. One view is that of the ocean as an integrator of the fast weather forcing, tentatively considered as random noise [e.g., *Hasselmann*, 1976; *Cessi*, 1994; *Pierini*, 2011, and references therein].

Conversely, a substantial body of work has been devoted to the understanding of the impact of the ocean on the atmosphere, in terms of contributing to generate atmospheric LFV and of thus facilitating its long-term forecast [*Christoph et al.*, 2000; *Czaja and Frankignoul*, 2002; *D'Andrea et al.*, 2005; *Kravtsov et al.*, 2007; *Brachet et al.*, 2012; *Gastineau et al.*, 2013; *Maidens et al.*, 2013]. The latter works have revealed that the Atlantic Ocean definitely has an impact on the dynamics of the atmosphere, but that this impact is relatively weak, unless the resolutions used in both the oceanic forcing and the atmospheric response are both higher than is the case in most of these studies [*Feliks et al.*, 2004, 2007; *Minobe et al.*, 2008; *Feliks et al.*, 2016].

The connection between the North Atlantic Ocean's sea surface temperatures (SSTs) and the NAO has also been studied in reanalysis data sets [*Wang et al.*, 2004; *Mosedale et al.*, 2006], using the Granger causality principle. *Mosedale et al.* [2006], in particular, showed that over most of the basin it is the atmospheric forcing that drives the SST field but that the opposite is the case over and near the Gulf Stream front near Cape Hatteras.

These analyses indicate that the two subsystems do mutually influence each other. But the nature and the strength of this interaction are not yet well understood. The central question is to clarify whether the dynamics of the full system involves a truly coupled variability that would not appear in either subsystem in the absence of coupling. The latter state of affairs is well known to prevail, for instance, in the Tropical Pacific's interannual variability [*Philander*, 1990; *Dijkstra*, 2005; *Dijkstra and Ghil*, 2005].

The present work is a step toward resolving this question. On the one hand, *Timmermann et al.* [1998] described the possible presence of a coupled mode of variability on a time scale of the order of 35 years in an intermediate-order ocean-atmosphere model, in which sea surface temperature, sea surface salinity, the ocean transport, and the NAO are involved. On the other hand, *Frankcombe et al.* [2010] and *Frankcombe and Dijkstra* [2011] recently reviewed and analyzed multidecadal variability in observations and climate models for the North Atlantic Basin. These authors showed that two dominant LFV signals are present at periods of 20–30 years and 50–70 years; the first of these was found already by *Ghil and Vautard* [1991] in Northern Hemisphere data and by *Plaut et al.* [1995] in the 335 year Central England temperature record, while the second one was identified by *Schlesinger and Ramnakutty* [1994] in global data. Frankcombe and coauthors also suggested that the former is associated with the internal variability of the Atlantic Meridional Overturning Circulation and the latter with exchange processes between the Atlantic and Arctic Oceans.

In the present work, we demonstrate that the shorter one of these two periodicities is not a purely internal ocean mode but a coupled mode of variability of the ocean-atmosphere system. In doing so, we lean on the findings of *Vannitsem et al.* [2015], who documented the presence of multidecadal variability in both the ocean and atmospheric components of a low-order coupled ocean-atmosphere model through both a bifurcation analysis and numerical integrations. In their model, the multidecadal variability originates from a Hopf bifurcation that gives rise to a stable long periodic orbit, whose loss of stability as the thermal forcing increases leads to this orbit becoming the backbone of a chaotic attractor.

The period of this orbit is controlled by the depth of the ocean's mixed layer [*Vannitsem*, 2015], and it varies between roughly 10 years for deep mixed layers and 70 years for thin mixed layers, while the motions on the chaotic attractor are still dominated by the time scale of this orbit for a broad range of parameter values. Moreover, the coupling parameter C between the ocean and the atmosphere is inversely proportional to the depth H of the mixed layer, and thus, thin mixed layers favor LFV development in this model.

In order to figure out whether such coupled dynamics could arise in the actual, observed ocean-atmosphere system, we investigate LFV in the reanalysis data sets currently available at the European Centre for Medium-Range Weather Forecasts (ECMWF), namely, ERA-20C for the atmosphere and ORAS4 for the ocean. The former is a long homogeneous reanalysis based on the model assimilation of surface data sets for 1900–2010. The latter is an ocean reanalysis based on surface forcings and ocean observations for 1958–2010. In section 2, the data compiled over the North Atlantic are first projected onto the dominant Fourier modes of the unstable periodic orbit identified in the low-order model of *Vannitsem et al.* [2015].

In section 3, the dynamics in this subspace are analyzed using multichannel singular spectrum analysis (MSSA), known to be able to isolate dynamical modes in a set of observables [*Broomhead and King*, 1986; *Vautard and Ghil*, 1989; *Ghil et al.*, 2002; *Alessio*, 2016]. A clear LFV signal is found on the 25–30 year time scale in the coupled ocean-atmosphere system. The internal origin of the coupling is then investigated through a dynamical analysis based on the nonlinear forecasting approach of *Sugihara and May* [1990]; this approach allows us to evaluate causal interactions between the two components of the coupled system. Section 4 is then devoted to discussing the nature of this coupled dynamics.

2. Data Sets

In order to investigate the dynamics of the coupled system over the North Atlantic, we use reanalysis data sets from the ECMWF and project them onto Fourier modes that dominate the coupled ocean-atmosphere dynamics in a low-order coupled model [*Vannitsem et al.*, 2015; *Vannitsem*, 2015; *De Cruz et al.*, 2016].

2.1. Reanalysis Data

Since we are interested in midlatitude ocean-atmosphere coupling and in understanding the NAO, we focus on the North Atlantic Basin, defined here as the spherical-rectangle domain (45°W–5°W, 25°N–60°N). This rectangle covers almost all of the North Atlantic, except the tropical and polar regions.

The atmospheric data set is extracted from the ERA-20C reanalysis for the twentieth century generated by the ECMWF from 1900 to 2010, and it is available from the ERA-20C ECMWF Public Data Sets web interface, http://www.ecmwf.int/en/research/climate-reanalysis/era-20C. The geopotential field Φ at 500 hPa is only

used here for the time interval 1958–2010, for which ocean data are also available. At large scales, Φ is closely related to the stream function field ψ_a, which in turn yields the geostrophic wind (u, v) at midlatitudes,

$$u = -\frac{1}{f_0}\frac{\partial \Phi}{\partial y} = -\frac{\partial \psi_a}{\partial y}, \quad v = \frac{1}{f_0}\frac{\partial \Phi}{\partial x} = \frac{\partial \psi_a}{\partial x}; \tag{1}$$

see also *Feliks et al.* [2016]. As usual, (x, y) and (u, v) point eastward and northward, respectively.

The ocean data set, known as ORAS4, is an ECMWF reanalysis with updated corrections [*Balmaseda et al.*, 2013; *Poli et al.*, 2015] that covers the interval 1958–2010 on a monthly basis. Two fields are selected, the potential temperature at 15 m depth and the sea level. Other potential temperature fields close to the surface provide similar spatiotemporal characteristics. The sea level has been chosen as a proxy for the barotropic stream function field, assuming that the ocean's large-scale LFV properties are well approximated by quasi-geostrophic shallow water dynamics, i.e.,

$$u = -\frac{g}{f_0}\frac{\partial \eta}{\partial y}, \quad v = \frac{g}{f_0}\frac{\partial \eta}{\partial x}, \tag{2}$$

where η is the sea level and $g/f_0\ \eta$ is a stream function [e.g., *Ghil and Childress*, 1987; *Vallis*, 2006]. Another ocean reanalysis data set [*Sakov et al.*, 2012] was used but proved to be too short for our purposes.

The number of points in each time series discussed henceforth is equal to 636 months for the joint 53 year interval January 1958 to December 2010.

2.2. Phase Space Projections

The different fields presented above are projected on the two dominant Fourier modes—denoted F_1 and Φ_2—of the large-scale coupled ocean-atmosphere dynamics found in *Vannitsem et al.* [2015], as discussed in Text S1 of the supporting information (SI).

Figure 1 shows the temporal evolution of the monthly values of the projection of the geopotential at 500 hPa on the Fourier mode F_1 and the temperature and stream function fields in the ocean on the Fourier mode Φ_2; see Text S1 of the SI. A clear seasonal signal is present in all three time series; as expected, the seasonal cycle is largest for the geopotential. Superimposed on this signal, both high- and low-frequency variabilities are visible—with the LFV component largest, again as expected, for the two ocean variables.

These features are well-known characteristics of the large-scale atmospheric and oceanic fields, respectively. Note that the projection on the F_1 and Φ_2 modes removes automatically the trends associated with the increase of the spatial average, since these modes have spatial averages equal to 0. In other words, the filtering we are using removes the upward sea level and temperature trends present in the ocean data sets [see *Balmaseda et al.*, 2013].

The common variability between these three variables can be represented by plotting the trajectory of the point $\left(\psi_{a,1}(t), \psi_{o,2}(t), \text{and} T_{o,2}(t)\right)$ in the corresponding three-dimensional (3-D) phase space. Figure 2a displays this trajectory in the 3-D space in which each cross represents one specific month. Note that each of the three coordinate series has been centered and normalized by its standard deviation, but the seasonality is not removed and is still therefore part of the dynamics. The time-averaged spatial variances captured by these three variables are equal to 18%, 42%, and 51% of the total variance in the entire data set, respectively.

A clear dependence seems to emerge, with the geopotential variable $\psi_{a,1}(t)$ taking on larger values when the oceanic temperature $T_{o,2}(t)$ and stream function $\psi_{o,2}(t)$ are higher. But is this correlation coincidental or is it the signature of coupled dynamics between the ocean and the atmosphere? This is the central question of the present work.

To analyze the LFV in this 3-D subspace, we start by investigating the covariance $\mathbf{C}$ between the three variables $\psi_{a,1}(t)$, $\psi_{o,2}(t)$, and $T_{o,2}(t)$, which is given by

$$\mathbf{C} = \begin{pmatrix} 1 & 0.22 & 0.122 \\ 0.22 & 1 & 0.52 \\ 0.122 & 0.52 & 1 \end{pmatrix}, \tag{3}$$

with entries that are significant at the 99% level. Note that, if one uses the NAO index of *Hurrell* [1995] instead of the projected geopotential on mode F_1, the correlation with the ocean variables is substantially smaller,

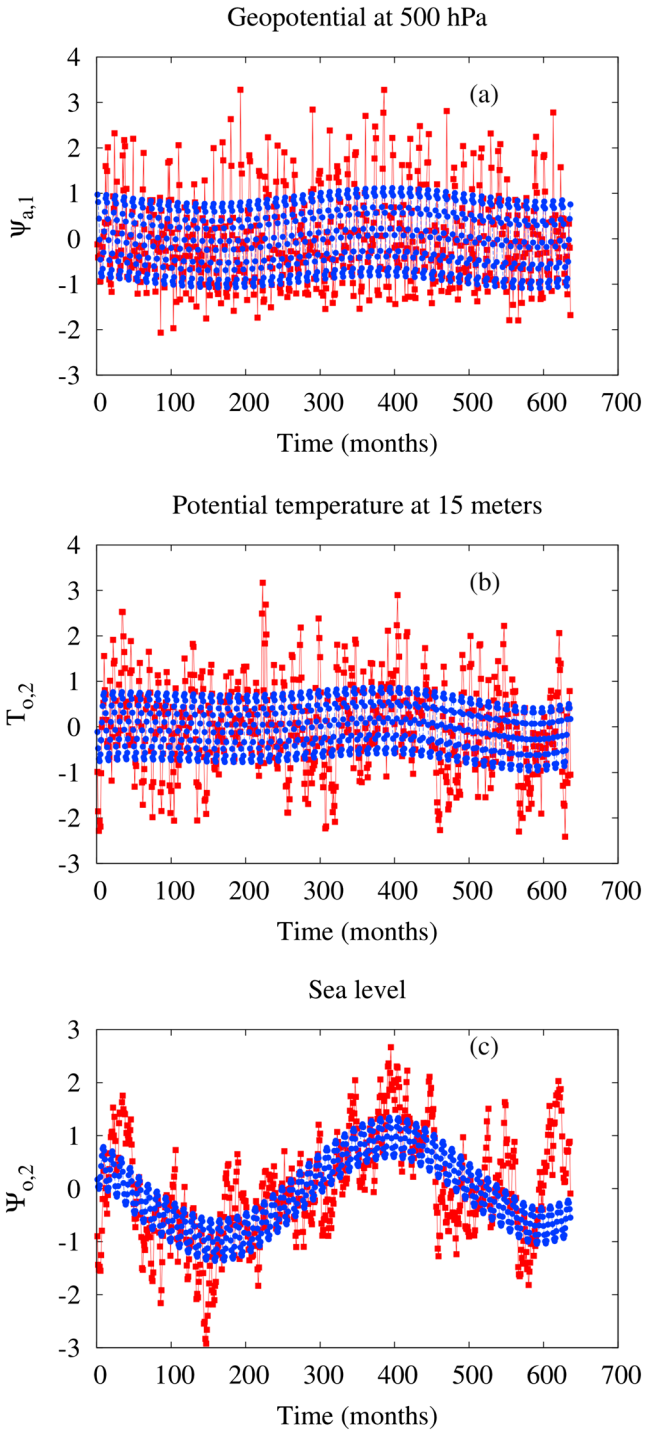

Figure 1. Time series of monthly means of the three variables selected for study; see Text S1 of the SI: (a) geopotential at 500 hPa projected on Fourier mode F_1, (b) potential temperature at 15 m depth projected on Fourier mode Φ_2, and (c) sea level projected on the same Fourier mode Φ_2. The time interval covered is the 636 months from January 1958 to December 2010; the monthly means are shown as red full squares and connected by straight red lines. The blue full circles correspond to the MSSA reconstruction using only the first four T-EOFs.

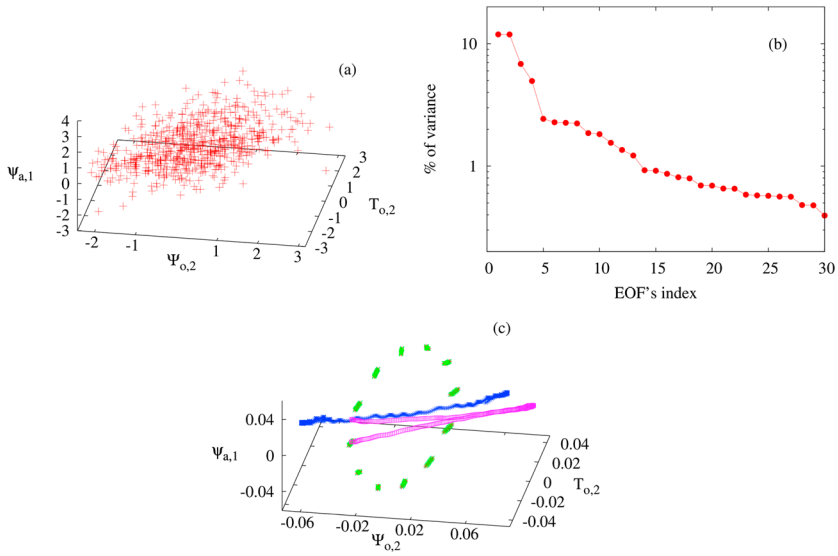

Figure 2. (a) Phase space representation of the evolution in time of the three variables plotted in Figure 1. Each cross now represents one monthly mean of the 3-D trajectory. (b) The variance captured by the first 30 T-EOFs resulting from the MSSA of the three variables displayed in Figure 2a. (c) Phase space representation of the leading four T-EOFs of the MSSA decomposition; the first two characterize the common seasonal variability embedded in the series, and the next pair, i.e., T-EOFs 3 and 4, captures the LFV that has a period of 25–30 years.

and it is significant at the 95% level only. This indicates that the NAO index might not necessarily be the most appropriate scalar index for studying the atmosphere's interaction with the ocean. This result supports our idea to focus on Fourier modes dominating the oceanic and atmospheric variability instead.

Equation (3) confirms that the covariability between the three variables under consideration is both high and statistically significant, but it does not reveal causality nor the origin of the common variability. In order to disentangle the causation between the variables and their common dynamics, other methods need to be brought to bear on the problem, as discussed, for instance, by *Sugihara et al.* [2012].

Two methods will be used in the present work: first MSSA, which has been successfully applied to investigate LFV in the atmosphere, ocean, and the coupled system [*Ghil et al.*, 2002, and references therein], and second the nonlinear forecasting method, which is adapted to the problem herein, in order to isolate the strength and orientation of the coupling between the variables under study.

3. Analysis of the LFV

3.1. The Modal Decomposition of the Coupled Variability

MSSA is based on the Karhunen-Loève decomposition of the lag-covariance matrix of a multivariate time series into an orthogonal set of eigenvectors—called temporal empirical orthogonal functions (T-EOFs), as opposed to the more common spatial EOFs (or S-EOFs) used in the climate sciences [e.g., *Preisendorfer*, 1988]—and the corresponding eigenvalues that equal the partial variance associated with the given S-EOF [*Ghil et al.*, 2002; *Alessio*, 2016]. The algorithm is briefly described in Text S2 of the SI.

This methodology is applied now to the three series discussed above with a time lag window of $M = 312$ months, i.e., 26 years. Given the length of the LFV time scales we are interested in, it is necessary to use such a large window, and *Groth and Ghil* [2015] have shown that this can be done while preserving statistical significance, provided that certain refinements are included in the algorithm. These refinements are now available in the freeware SSA-MTM Toolkit at https://dept.atmos.ucla.edu/tcd/ssa-mtm-toolkit.

The variance captured by each T-EOF is shown in Figure 2b. Three groups of eigenvalues are well separated. Two pairs of eigenvalues—1 + 2 and 3 + 4—rise above the background: they capture 22% and 12% of the total variance, respectively. The corresponding T-EOFs are plotted in Figure 2c in the same 3-D phase space as the data in Figure 2a. The third group is often referred to as the continuous background or the tail of the eigenvalue distribution.

The first and second EOFs describe a smooth ellipse in the 3-D subspace, and they are clearly associated with the seasonal variability present in the three time series. This pair captures more than one fifth of the variability in our 3-D subspace. The third and fourth EOFs display a very different structure with a slow evolution along an almost straight line, starting from low values of all three variables, attaining their largest values after roughly half of the time lag window $M = 26$ years used in the MSSA, and then back to smaller values. The typical period of the associated LFV is of the order of 25–30 years, as found by *Timmermann et al.* [1998] and *Frankcombe et al.* [2010].

The reconstruction of the three variables based on the first four EOFs is shown by the blue lines in Figures 1a–1c. The LFV associated with EOF pair (3,4) is dominating the variability of the ocean transport in Figure 1c, and it is less pronounced for the other two variables. Still, this pair does capture a weak modulation of the variability on the same long time scale in both ocean temperature and atmospheric zonal transport; see Figures 1a and 1b, respectively.

To check whether the slow variability captured by the EOF pair (3,4) is statistically significant or not, we first applied the χ^2 test and the Monte Carlo approach of the SSA-MTM Toolkit. Given the shortness of the data sets, these tests only indicated a significance level below 95%.

To ascertain the importance of the LFV detected by the analysis, we propose instead the following random shuffling test: perform the same analysis on the three series $X_1(t) = \psi_{a,1}(t)$, $X_2(t) = T_{o,2}(t)$, and $X_3(t) = \psi_{o,2}(t)$ that are, however, shifted left in time by a random number of whole years, while the disregarded years are added at the right end of the series. Applying MSSA with the same window width M, the intermediate pair of eigenvalues (3,4) of Figure 2b is now part of the background variability; cf. Figure S1 in the SI. This result confirms that the pair (3,4) is indeed significant and describes a coherent joint LFV among the three variables.

To summarize, these diagnostic results suggest that a coupled LFV mode is present in the ocean-atmosphere system, as viewed through the reanalysis data sets used herein and through the prism of the three large-scale variables selected according to the modeling results of *Vannitsem et al.* [2015]. It is interesting to note that the near periodicity of 25–30 years that characterizes this emerging LFV is also present in each of the three individual time series. This multidecadal near periodicity is masked, however, in each one of them by many other signals: at 20 years, 15 years, and subseasonal periodicities for the geopotential at 500 hPa in the atmosphere and at 10–15 years, 4–6 years, and subseasonal periodicities for the temperature and sea level in the ocean (not shown). The greater prominence of the 25–30 year signal in the joint MSSA of our three variables suggests that this LFV signal is closely associated with their joint dynamics. This result, however, does still not help us decide whether the joint multidecadal variability is due to an external forcing or to internal mechanisms.

In order to evaluate whether the dynamics is associated with the coupling between the variables, we propose next a score based on the nonlinear forecasting method.

3.2. Inference of the Coupling Intensity Based On Analog Dynamics

In the 1990s, a new data-driven approach to nonparametric and nonlinear forecasting was formulated [*Casdagli*, 1989; *Sugihara and May*, 1990; *Tsonis*, 1992]. The main idea is to use past forecasts to infer the future of the current state of a system, provided that past initial states can be found sufficiently close to the actual situation. These close situations are known as analogs and have been used extensively in studying atmospheric predictability [*Lorenz*, 1969; *Toth*, 1991; *Trevisan*, 1995; *Nicolis*, 1998] or for the purposes of downscaling [*Hamill and Whitaker*, 2006, and references therein].

In high-dimensional problems, applying this approach requires one to first embed the problem into a low-dimensional subspace by using the Mañé-Takens method of delays applied to a single time series [*Broomhead and King*, 1986; *Tsonis*, 1992, and references therein]. In the present case, a 3-D phase space is already defined by the three variables (X_1, X_2, and X_3) discussed earlier, and one can focus on the forecasting problem in this 3-D space. The technical aspects of selecting the analogs are provided in Text S3 of the SI.

Let us now denote the L forecasts from an initial time t_0 by $\mathbf{X}^{(l)}(t;t_0) = \left(X_i^{(l)}(t;t_0)\right)$, where $i = 1, 2, 3$ labels the components of the state vector in the 3-D space and $l = 1, \ldots, L$ labels the analogs used at t_0. The value of L is fixed to $L = D+1$, where $D = 3$ is the dimension of the space, as discussed in Text S3 of the SI. The forecasting system is then given by

$$\mathbf{Y}(t) = \sum_{l=1}^{L} w_l \mathbf{X}^{(l)}(t;0)\,, \tag{4}$$

where t is the lead time, $t_0 = 0$ for convenience, and the weights w_l given to each analog are equal to $w_l = \exp\left(-d(\mathbf{X}(0), \mathbf{X}^{(l)}(0,0))\right) / \sum_l \exp\left(-d(\mathbf{X}(0), \mathbf{X}^{(l)}(0,0))\right)$, with $d(X(0), X^{(l)}(0,0))$ the distance between the reference initial state $\mathbf{X}(t_0 = 0)$ and the analog $\mathbf{X}^{(l)}(0,0)$.

Note that the distance d can de defined either in the 3-D space, as done in equation (4) above, in which case one takes into account the dynamics on the system's attractor. But it can also be defined for each individual variable i, assuming that the variables are independent; the latter choice will presumably lead to a different selection of analogs. If the two approaches lead to a very similar error evolution, then one can conclude that there is no coupling between the three variables selected above, i.e., there is no information flowing from one individual variable to the others.

On the contrary, if the error dynamics is markedly different between the two approaches, and if the errors are smaller in the 3-D case, it means that coupling is present between the variables—a fact that is taken into account while measuring the distance in the 3-D phase space—and that this coupling can improve the forecast skill. A detailed analysis of the skill of the different variables is given in Text S4 of the SI. This analysis suggests that some improvement of skill is present when the three variables are combined, instead of each variable being treated separately.

3.3. The Skill Dependence Score

Due to the short length of the time series, however, large sampling errors are present, and care should be taken in infering coupling. A more quantitative measure of the interdependence between the variables is given by the Skill Dependence Score (SDS). This score is defined herein by

$$\mathrm{SDS} = 1 - \frac{\mathrm{MSE}_{\mathrm{Dep}}}{\mathrm{MSE}_{\mathrm{Ind}}}, \tag{5}$$

where MSE is mean square error and $\mathrm{MSE}_{\mathrm{Dep}}$ is the measure of the error when interdependences are taken into account, while $\mathrm{MSE}_{\mathrm{Ind}}$ corresponds to the same measure when the interdependences are supposed to be absent. In principle, if $\mathrm{SDS} > 0$, the interdependence of the set of variables considered should be accepted.

In practice, one needs to evaluate the statistical significance of the SDS, which requires one to estimate the uncertainty in both $\mathrm{MSE}_{\mathrm{Dep}}$ and $\mathrm{MSE}_{\mathrm{Ind}}$. For $\mathrm{MSE}_{\mathrm{Dep}}$, a simple way to evaluate the uncertainty associated with the limited sample present in the current analysis is to use a bootstrap method [*Efron and Tibshirani*, 1993] by randomly selecting a new set of S forecast error evolutions out of the S original ones; in doing so, a specific error evolution can be selected several times or completely disregarded. The number of forecasts for each season is $3 \times (53-8)$ years $= 135$. Note that 4 years is disregarded at the beginning and the end of the series for the selection of initial forecast dates, in order to keep the same number of points in the pool of potential analogs.

For the $\mathrm{MSE}_{\mathrm{Ind}}$, one can perform a certain number of times the forecast experiment presented above by randomly shuffling the three time series, as already done in evaluating the significance of the LFV found by MSSA, but keeping the selection of the analogs in the 3-D space. The shuffling removes the coherent 25–30 year signal, along with any other signals at interannual time scales.

We performed 1000 realizations of these shuffling experiments and computed for each of them the SDS, followed by computing the mean and standard deviation of the ensemble. Since SDS has a unimodal distribution, one can use a Gaussian assumption to evaluate the significance of the SDS values computed. The averaged SDS (red filled circles) and its two-sided confidence interval at the 95% level (light dotted red lines) are plotted in Figure 3 for boreal winter.

An alternative way to evaluate the SDS is to compute the $\mathrm{MSE}_{\mathrm{Ind}}$ obtained by considering separately each variable, as if they were independent, while keeping the same number of analogs as for $\mathrm{MSE}_{\mathrm{Dep}}$. The results of this calculation are plotted as the blue filled triangles in Figure 3.

Interestingly, the variations in this version of the score follow closely those obtained in the shuffling experiment version, suggesting that the results of our analysis are robust. A remarkable result is the positive value of SDS when the forecasts are started in winter: in particular, highly significant positive values occur in the forecasts for the subsequent summer, for geopotential at 500 hPa at lead times of 5–6 months, 16–17 months, and (surprisingly) 41–42 months; for potential temperature at 15 months although quite marginal so; and for sea level at 5–6 months and at 14–17 months. This finding indicates that the three fields are coupled at large scales in winter and that this feature can be exploited in forecasts for the North Atlantic that are

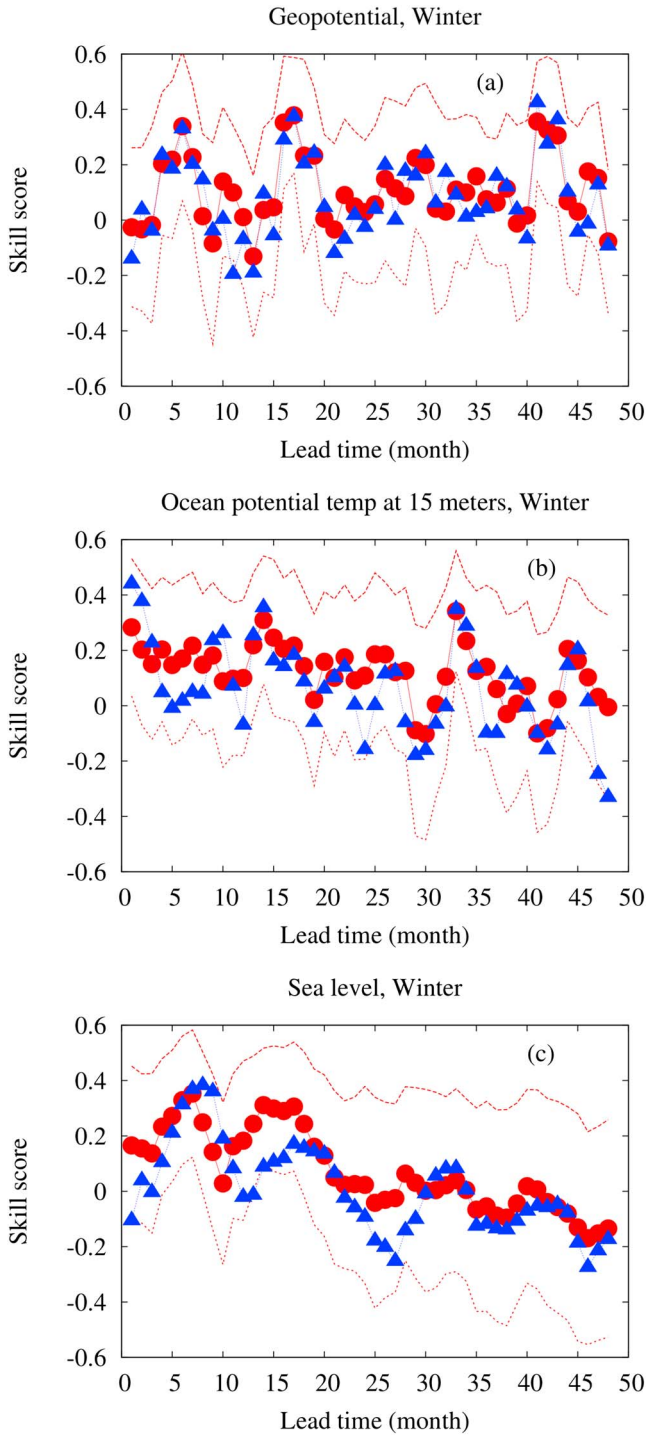

Figure 3. Evolution with lead time of the Skill Dependence Score (SDS), as defined in equation (5), for analog-based forecasts that are initialized in winter (December-January-February), as calculated for (a) $X_1 = \psi_{a,1}$, (b) $X_2 = T_{o,2}$, and (c) $X_3 = \psi_{o,2}$. The SDS is computed in two different ways (red filled circles versus blue filled triangles), and the two-sided confidence interval at 95% is shown for one of the two; see text for details.

initialized in winter. In other words, knowing the initial state in this 3-D subspace in winter improves long-term forecasts.

When starting forecasts in summer (Figure S5), the SDS is significantly positive for the geopotential at the end of autumn and in early winter, at a lead time of 4–5 months, while its values for the other two variables are not as significant. This finding suggests that the coupling in summer is more unidirectional than in winter. Such a greater unidirectionality could be associated with the small depth of the mixed layer in summer, which modifies the heat exchanges between the two subsystems and hence the strength of the coupling.

The SDS evolution for spring and autumn is provided in Figures S6 and S7. When initializing forecasts during these transition seasons, the only significantly positive SDS values occur for the sea level variable and the significance is higher when forecasts are started in autumn. The impact upon extended-range predictability of initializing the ocean versus the atmosphere or both during the transition seasons thus deserves further investigation.

These results suggest that the influence of the coupling on the dynamics varies as a function of the season. The reason for this specific seasonal pattern of the coupling is not yet clear, and further analyses need to be performed, in particular, by considering longer time series that can provide closer analogs, and by using additional approaches for disentangling causality [*Sugihara et al.*, 2012; *Deza et al.*, 2015; *Jajcay et al.*, 2016], and also through the analysis of the same variables in more detailed coupled ocean-atmosphere models.

4. Discussion

We investigated the coupling between the ocean and the atmosphere over the North Atlantic based on geopotential at 500 hPa, ocean temperatures at 15 m depth, and sea level heights; these fields were extracted from an atmospheric and an oceanic reanalysis data set. After projecting these fields onto two dominant Fourier modes of the ocean and atmosphere, the mutual dependence between the three resulting time series was explored using two separate approaches: (i) multichannel singular spectrum analysis (MSSA) [*Ghil et al.*, 2002, and references therein] and (ii) the nonparametric, nonlinear forecasting approach of *Sugihara and May* [1990]. The statistical approach (i) gave information on the dominant low-frequency variability (LFV) shared by the three time series, while the dynamical approach (ii) lead to information on the predictability of the coupled system. The latter approach was adapted to build a Skill Dependence Score (SDS) in order to assess the impact of the coupling between the variables under investigation upon predictability.

We found a dominant LFV mode with a time scale of 25–30 years, already identified by *Frankcombe et al.* [2010] for the ocean only. The present analysis indicates that this LFV mode is common to the ocean and the atmosphere, suggesting coupled dynamics of the two fluid media, as described by *Vannitsem et al.* [2015]. The computation of the SDS further suggests that the coupled dynamics has a pronounced impact on the predictability of ocean-atmosphere system.

Note that the coupling found using the SDS could be associated with other long-term signals, from interannual to multidecadal time scales. Still given the dominance of the 25–30 year signal for the coupled ocean-atmosphere dynamics revealed by the MSSA, we suspect that the increased predictability is due to this specific long-term signal.

Neither of the two approaches, statistical nor dynamical, allows one to determine the specific nature of the coupled LFV mode. Note that resolving this issue is not a purely theoretical problem but could have important implications in terms of the climate system's predictability.

As shown by *Vannitsem et al.* [2015], the presence or absence of a truly coupled slow mode leads to very different error dynamics: within a range of model parameters in which the solution is a slow periodic limit cycle or even a "fuzzy" slow manifold that is fully coupled, error growth is on the time scale of this slow, LFV behavior. Once rapid atmospheric modes become decoupled, error growth is much faster and predictability deteriorates sharply.

Vannitsem and Lucarini [2016] have confirmed that—when the atmosphere is in a structurally stable regime and it is only weakly affected by the ocean—error growth is rapid, while the error dynamics is synchronized between the atmosphere and ocean for long lead times when the coupled LFV mode sets in, leading to potential long-term forecasts for the atmosphere as well. Disentangling the very nature of the coupled dynamics,

beyond the classical correlation and teleconnection approaches, is therefore a crucial issue, whose resolution should help clarify our ability to make long-term forecasts or not.

For the real ocean-atmosphere system, it is hard to get such information since we cannot arbitrarily modify the parameters of the system, e.g., the surface friction coefficient, as done in the two above mentioned theoretical papers [*Vannitsem et al.*, 2015; *Vannitsem and Lucarini*, 2016]. This question is therefore difficult to answer using observational data sets, and one must rely on the dynamics generated in coupled models of increasing complexity, as suggested in *Ghil* [2017, and references therein]. *Vannitsem et al.* [2015] have started such an analysis, and it will be extended to more complicated coupled systems, like the one recently developed by *De Cruz et al.* [2016].

Acknowledgments

It is a pleasure to thank L. Bertino and J. Xie for enlightening discussions. This work is partially supported by the Belgian Science Policy Office under contract BR/121/A2/STOCHCLIM (SV). M.G. gratefully acknowledges support by grant N00014-16-1-2073 from the Multidisciplinary University Research Initiative (MURI) of the Office of Naval Research and by the National Science Foundation grant OCE-1243175. The projected data produced for this work are available from the authors.

References

Alessio, S. M. (2016), *Digital Signal Processing and Spectral Analysis for Scientists: Concepts and Applications*, 900, Springer, Switzerland.

Baehr, J., et al. (2015), The prediction of surface temperature in the new seasonal prediction system based on the MPI-ESM coupled climate model, *Clim. Dyn.*, *44*, 2723–2735.

Balmaseda, M. A., K. Morgensen, and A. T. Weaver (2013), Evaluation of the ECMWF ocean reanalysis system ORAS4, *Q. J. R. Meteorol. Soc.*, *139*, 1132–1161.

Bladé, I., B. Liebmann, D. Fortuny, and G.-J. van Oldenborgh (2011), Observed and simulated impacts of the summer NAO in Europe: Implications for projected drying in the Mediterranean region, *Clim. Dyn.*, *39*, 709–727, doi:10.1007/s00382-011-1195-x.

Brachet, S., F. Codron, Y. Feliks, M. Ghil, H. Le Treut, and E. Simonnet (2012), Atmospheric circulations induced by a midlatitude SST front: A GCM study, *J. Clim.*, *25*, 1847–1853.

Broomhead, D. S., and G. P. King (1986), Extracting qualitative dynamics from experimental data, *Physica D*, *20*, 217–236.

Casdagli, M. (1989), Nonlinear prediction of chaotic time series, *Physica D*, *35*, 335–356.

Cessi, P. (1994), A simple box model of stochastically forced thermohaline flow, *J. Phys. Oceanogr.*, *24*, 1911–1920.

Christoph, M., U. Ulibrich, J. M. Oberhuber, and E. Roeckner (2000), The role of ocean dynamics for low-frequency fluctuations of the NAO in a coupled ocean-atmosphere GCM, *J. Clim.*, *13*, 2536–2549.

Czaja, A., and C. Frankignoul (2002), Observed impact of Atlantic SST anomalies on the North Atlantic Oscillations, *J. Clim.*, *15*, 606–623.

D'Andrea, F., A. Czaja, and J. Marshall (2005), Impact of anomalous ocean heat transport on the North Atlantic Oscillation, *J. Clim.*, *18*, 4955–4969.

De Cruz, L., J. Demaeyer, and S. Vannitsem (2016), A modular arbitrary-order ocean-atmosphere model: MAOOAM v1.0, *Geosci. Model Dev.*, *9*, 2793–2808, doi:10.5194/gmd-2016-59.

Deza, J., M. Barreiro, and C. Masoller (2015), Assessing the direction of climate interactions by means of complex networks and information theoretic tools, *Chaos*, *25*, 033105.

Dijkstra, H. A. (2005), *Nonlinear Physical Oceanography: A Dynamical Systems Approach to the Large Scale Ocean Circulation and El Niño* 2nd ed., Springer, New York.

Dijkstra, H. A., and M. Ghil (2005), Low-frequency variability of the large-scale ocean circulation: A dynamical systems approach, *Rev. Geophys.*, *43*, RG3002, doi:10.1029/2002RG000122.

Efron, B., and R. Tibshirani (1993), *An Introduction to the Bootstrap*, p. 436, Chapman and Hall, New York.

Feliks, Y., M. Ghil, and E. Simonnet (2004), Low-frequency variability in the midlatitude atmosphere induced by an oceanic thermal front, *J. Atmos. Sci.*, *61*, 961–981.

Feliks, Y., M. Ghil, and E. Simonnet (2007), Low-frequency variability in the midlatitude baroclinic atmosphere induced by an oceanic thermal front, *J. Atmos. Sci.*, *64*, 97–116.

Feliks, Y., A. W. Anderson, and M. Ghil (2016), Interannual variability in North Atlantic weather: Data analysis and a quasi-geostrophic model, *J. Atmos. Sci*, *73*, 3227–3247.

Frankcombe, L. M., A. von der Heydt, and H. A. Dijkstra (2010), North Atlantic multidecadal climate variability: An investigation of dominant time scales and processes, *J. Clim.*, *23*, 3626–3638.

Frankcombe, L. M., and H. A. Dijkstra (2011), The role of Atlantic-Arctic exchange in North Atlantic multidecadal climate variability, *Geophys. Res. Lett.*, *38*, L16603, doi:10.1029/2011GL048158.

Gastineau, G., F. D'Andrea, and C. Frankignoul (2013), Atmospheric response to the North Atlantic Ocean variability on seasonal to decadal time scales, *Clim. Dyn.*, *40*, 2311–2330.

Ghil, M. (2017), The wind-driven ocean circulation: Applying dynamical systems theory to a climate problem, *Discrete Cont. Dyn. Syst. A*, *37*(1), 189–228, doi:10.3934/dcds.2017008.

Ghil, M., and S. Childress (1987), *Topics in Geophysical Fluid Dynamics: Atmospheric Dynamics, Dynamo Theory and Climate Dynamics*, p. 485, Springer, New York.

Ghil, M., and R. Vautard (1991), Interdecadal oscillations and the warming trend in global temperature time series, *Nature*, *350*(6316), 324–327.

Ghil, M., et al. (2002), Advanced spectral methods for climate time series, *Rev. Geophys.*, *40*(1), 1003, doi:10.1029/2000RG000092.

Groth, A., and M. Ghil (2015), Monte Carlo singular spectrum analysis (SSA) revisited: Detecting oscillator clusters in multivariate datasets, *J. Clim.*, *19*, 7873–7893.

Hamill, T. M., and J. S. Whitaker (2006), Probabilistic quantitative precipitation forecasts based on reforecast analogs: Theory and application, *Mon. Weather Rev.*, *134*, 3209–3229.

Hasselmann, K. (1976), Stochastic climate models. Part I: Theory, *Tellus*, *28*, 473–485.

Hurrell, J. (1995), Decadal trends in the North Atlantic Oscillation: Regional temperatures and precipitation, *Science*, *269*(5224), 676–679, doi:10.1126/science.269.5224.676.

Hurrell, J. W., Y. Kushnir, G. Ottersen, and M. Visbeck (2013), *The North Atlantic Oscillation: Climatic Significance and Environmental Impact, Geophys. Monogr. Ser.*, AGU, Washington, D. C., doi:10.1029/GM134.

Jajcay, N., J. Hlinka, S. Kravtsov, A. A. Tsonis, and M. Palus (2016), Time scales of the European surface air temperature variability: The role of the 7–8 year cycle, *Geophys. Res. Lett.*, *43*, 902–909, doi:10.1002/2015GL067325.

Kadow, C., et al. (2015), Evaluation of forecasts by accuracy and spread in the MiKlip decadal climate prediction system, *Meteorol. Z.*, *25*, 631–643, doi:10.1127/metz/2015/0639.

Kravtsov, S., W. K. Dewar, P. Berloff, M. Ghil, and J. C. McWilliams (2007), A highly nonlinear coupled mode of decadal variability in a mid-latitude ocean-atmosphere model, *Dyn. Atmos. Oceans*, *43*, 123–150.
Lorenz, E. N. (1969), Atmospheric predictability as revealed by naturally occuring analogs, *J. Atmos. Sci.*, *26*, 636–646.
Maidens, A., A. Arribas, A. A. Scaife, C. MacLachlan, D. Peterson, and J. Knight (2013), The influence of surface forcings on prediction of the North Atlantic Oscillation regime of winter 2010/2011, *Mon. Weather Rev.*, *141*, 3801–3813.
Menary, M., D. Hodson, J. Robson, R. Sutton, and R. Wood (2015), A mechanism of internal decadal variability in a high resolution coupled climate model, *J. Clim.*, *28*, 7764–7785, doi:10.1175/JCLI-D-15-0106.1.
Minobe, S., A. Kuwano-Yoshida, N. Komori, S. P. Xie, and R. J. Small (2008), Influence of the Gulf Stream on the troposphere, *Nature*, *452*, 206–209.
Mosedale, T., D. Stephenson, M. Collins, and T. Mills (2006), Granger causality of coupled climate processes: Ocean feedback on the North Atlantic Oscillation, *J. Clim.*, *19*, 1182–1194.
Nicolis, C. (1998), Atmospheric analogs and recurrence time statistics: Toward a dynamical formulation, *J. Atmos. Sci.*, *55*, 465–475.
Philander, S. G. H. (1990), *El Niño and the Southern Oscillation*, Academic Press, New York.
Pierini, S. (2011), Low-frequency variability, coherence resonance, and phase selection in a low-order model of the wind-driven ocean circulation, *J. Phys. Oceanogr.*, *41*, 1585–1604.
Plaut, G., M. Ghil, and R. Vautard (1995), Interannual and interdecadal variability in 335 years of Central England temperatures, *Science*, *268*, 710–713.
Poli, P., et al. (2015), The data assimilation system and initial performance evaluation of the ECMWF pilot reanalysis of the 20th-century assimilating surface observations only, ERA Rep. Seri., p. 14, European Cent. for Medium-range Weather Forecasts, Reading, U. K.
Preisendorfer, R. W. (1988), *Principal Component Analysis in Meteorology and Oceanography*, 425 pp., Elsevier, New York.
Sakov, P., F. Counillon, L. Bertino, K. A. Lisaeter, P. R. Oke, and A. Korablev (2012), TOPAZ4: An ocean-sea ice data assimilation system in the North Atlantic and Arctic Ocean, *Science*, *8*, 633–656.
Schlesinger, M. E., and N. Ramnakutty (1994), An oscillation in the global climate system of period 65–70 years, *Nature*, *367*(6465), 723–726.
Sugihara, G., and R. M. May (1990), Nonlinear forecasting as a way of distinguishing chaos from measurement error in time series, *Nature*, *344*, 734–741.
Sugihara, G., R. May, H. Ye, C-H. Hsieh, E. Deyle, M. Fogarty, and S. Munch (2012), Detecting causality in complex ecosystems, *Science*, *338*, 496–500.
Timmermann, A., M. Latif, R. Voss, and A. Grotzner (1998), Northern hemispheric interdecadal variability: A coupled air-sea mode, *J. Clim.*, *11*, 1906–1930.
Toth, Z. (1991), Estimation of atmospheric predictability by circulation analogs, *Mon. Weather Rev.*, *119*, 65–72.
Tsonis, A. A. (1992), *Chaos: From Theory to Applications*, 278 pp, Springer, New York.
Trevisan, A. (1995), Statistical properties of predictability from atmospheric analogs and the existence of multiple flow regimes, *J. Atmos. Sci.*, *52*, 3577–3592.
Vallis, G. (2006), *Amospheric and Oceanic Fluid Dynamics*, 745 pp., Cambridge Univ. Press, Cambridge, U. K.
Vannitsem, S. (2015), The role of the ocean mixed layer on the development of the North Atlantic Oscillation: A dynamical system's perspective, *Geophys. Res. Lett.*, *42*, 8615–8623, doi:10.1002/2015GL065974.
Vannitsem, S., and V. Lucarini (2016), Statistical and dynamical properties of covariant Lyapunov vectors in a coupled atmosphere-ocean model—Multiscale effects, geometric degeneracy, and error dynamics, *J. Phys. A*, *49*, 224001.
Vannitsem, S., J. Demaeyer, L. de Cruz, and M. Ghil (2015), Low-frequency variability and heat transport in a low-order nonlinear coupled ocean-atmosphere model, *Physica D*, *309*, 71–85.
Vautard, R., and M. Ghil (1989), Singular spectrum analysis in non-linear dynamics, with applications to paleoclimatic time series, *Physica D*, *35*, 395–424.
Wang, W., B. T. Anderson, R. K. Kaufmann, and R. B. Myneni (2004), The relation between the North Atlantic Oscillation and SSTs in the North Atlantic Basin, *J. Clim.*, *17*, 4752–4759.